THE JOURNAL OF BIOLOGICAL CHEMISTRY VOL. 288, NO. 4, pp. 2452–2463, January 25, 2013

The V499G/Y501H Mutation Impairs Fast Motor Kinetics of Prestin and Has Significance for Defining Functional Independence of Individual Prestin Subunits*[S]

Received for publication, August 17, 2012, and in revised form, November 8, 2012 Published, JBC Papers in Press, December 4, 2012, DOI 10.1074/jbc.M112.411579

Kazuaki Homma[‡1], **Chongwen Duan**[‡], **Jing Zheng**[‡§], **Mary Ann Cheatham**[§¶], **and Peter Dallos**[§¶‖]

From the [‡]*Department of Otolaryngology-Head and Neck Surgery, Feinberg School of Medicine, Northwestern University, Chicago, Illinois 60611 and* [§]*The Hugh Knowles Center for Clinical and Basic Science in Hearing and Its Disorders and Departments of* [¶]*Communication Sciences and Disorders and* [‖]*Neurobiology, Northwestern University, Evanston, Illinois 60208*

Background: Prestin converts electrical energy into mechanical work.
Results: The V499G/Y501H mutation significantly impairs fast motor kinetics of prestin.
Conclusion: Impaired kinetics is attributable to mutation at the Val-499 site that is conserved among SLC26 proteins regardless of their function as motors or transporters.
Significance: V499G/Y501H mutated prestin provides clues to the molecular mechanisms underlying somatic electromotility and thus cochlear amplification.

Outer hair cells (OHCs) are a mammalian innovation for mechanically amplifying sound energy to overcome the viscous damping of the cochlear partition. Although the voltage-dependent OHC membrane motor, prestin, has been demonstrated to be essential for mammalian cochlear amplification, the molecular mechanism by which prestin converts electrical energy into mechanical displacement/force remains elusive. Identifying mutations that alter the motor function of prestin provides vital information for unraveling the energy transduction mechanism of prestin. We show that the V499G/Y501H mutation does not deprive prestin of its voltage-induced motor activity, but it does significantly impair the fast motor kinetics and voltage operating range. Furthermore, mutagenesis studies suggest that Val-499 is the primary site responsible for these changes. We also show that V499G/Y501H prestin forms heteromers with wild-type prestin and that the fast motor kinetics of wild-type prestin is not affected by heteromer formation with V499G/Y501H prestin. These results suggest that prestin subunits are individually functional within a given multimer.

The mammalian cochlea has two classes of hair cells with distinct morphology, innervation, and physiological functions. Inner hair cells are presumed to be sensory, mechanoreceptor cells that convert sound-induced mechanical stimuli into electric signals that ultimately excite afferent neurons. In contrast, outer hair cells (OHCs)[2] are primarily specialized for amplifying sound energy that would otherwise dissipate due to viscous damping in the cochlea. The membrane-based motor protein prestin confers voltage-induced, cell length change onto OHCs (1). The indispensability of this prestin-based OHC electromotility to normal cochlear amplification was demonstrated by a series of studies (2–5).

Changes in transmembrane electrical potential induce charge displacement in prestin that is converted into mechanical displacement/force. Growing evidence suggests that the voltage sensor(s) of prestin is intrinsic (6–8). However, it remains unclear how prestin converts electrical energy into mechanical work and why this energy transduction process only occurs in mammalian and platypus prestins and not in non-mammalian prestin orthologs (9, 10). Although prestin multimers (11–15) could serve as minimal motor units, the functional significance of multimer formation is not clear. Functional analyses of mutated prestins whose motor functions are augmented or attenuated in various ways provide clues for unraveling the energy transduction mechanism of prestin. A careful examination of the motor properties of various prestin mutations must, therefore, be undertaken to understand the evolution of electromotile performance in prestin, which is the only member of the solute carrier family (SLC26) with this capability. In contrast to prestin (SLC26A5), most other family members function as transporters.

V499G/Y501H prestin (abbreviated as 499-prestin) (16) is a fortuitously generated mutant that successfully targets the lateral membrane so that normal OHC morphology is maintained, but its motor function at physiologically relevant membrane potentials is reduced due to a significantly depolarized voltage operating point (5). A knockin mouse model expressing 499-prestin shows a decrease in hearing sensitivity and thereby serves as a more appropriate model for demonstrating the contribution of prestin-based OHC electromotility to mammalian cochlear amplification compared with prestin knock-out mice (5). In these latter mouse models, OHCs show significant morphological and axial stiffness changes due to the absence of

* This work was supported, in whole or in part, by National Institutes of Health Grants DC00089 (to P. D.) and DC010633 (to J. Z.). This work was also supported by The Hugh Knowles Center.
[S] This article contains supplemental Figs. S1–S4.
[1] To whom correspondence should be addressed: Dept. of Otolaryngology-Head and Neck Surgery, Feinberg School of Medicine, Northwestern University, 303 E. Chicago Ave., Chicago, IL 60611. Tel.: 312-503-5344; E-mail: k-homma@northwestern.edu.
[2] The abbreviations used are: OHC, outer hair cell; NLC, nonlinear capacitance; 499-prestin, V499G/Y501H prestin; het, heterozygote; ki, knockin; AICc, corrected Akaike Information Criterion; fC, femtocoulomb(s); pF, picofarad(s).

prestin protein expression in the lateral membrane (2–5). These changes could by themselves result in a loss of gain independent of whether prestin is associated with cochlear amplification or not.

In this report, we highlight the motor properties of 499-prestin to gain insights as to how motor function is affected by the V499G/Y501H mutation. The Val-499/Tyr-501 site of prestin is predicted to reside near the C-terminal end of the last transmembrane segment immediately preceding its intracellular C-terminal domain (see "Results"). Because this region is highly conserved among SLC26 family members, these two amino acids were not expected to correlate with motor function, which is unique to prestin. Hence, the drastic change in electromotility by the V499G/Y501H mutation was unexpected and required comprehensive characterization. This report demonstrates that the fast motor kinetics of prestin is significantly impaired by the mutation. We also show that 499-prestin forms heteromers with wild-type prestin, which allows us to study how individual prestin subunits contribute to the overall motor properties of prestin multimers. Our results suggest that the changes in motor properties found in V499G/Y501H prestin are attributable to V499G alone and that the motor function of prestin is not affected by multimer formation, suggesting functional independence of prestin subunits within multimers.

EXPERIMENTAL PROCEDURES

Hair Cell Preparation and in Vitro Electrophysiology—Adult mice were euthanized with Euthasol (200 mg/kg), and OHCs were isolated as described previously (17). Whole-cell recordings were performed at room temperature using the Axopatch 200B amplifier (Molecular Devices, Sunnyvale, CA). Recording pipettes were pulled from borosilicate glass to achieve initial bath resistances averaging 3–4 megaohms. Whole-cell nonlinear capacitance (NLC) recordings were performed using a 0-mV holding potential and a sinusoidal voltage stimulus (2.5 Hz, 120-mV amplitude) superimposed with two higher frequency stimuli (390.6 (f_1) and 781.3 (f_2) Hz, 10-mV amplitude throughout the study unless otherwise specified. For stimulus frequency-dependent NLC measurements, f_1 was set at 195.3 (f_2 = 390.6), 390.6 (f_2 = 781.3), 781.3 (f_2 = 1563), 1563 (f_2 = 3125), and 3125 (f_2 = 6250) Hz. Recording pipettes were filled with an intracellular solution containing 140 mM CsCl, 2 mM $MgCl_2$, 10 mM EGTA, and 10 mM HEPES (pH 7.3). Cells were bathed in an extracellular solution containing 120 mM NaCl, 20 mM tetraethylammonium chloride, 2 mM $CoCl_2$, 2 mM $MgCl_2$, 10 mM HEPES (pH 7.3). Osmolarity was adjusted to 310 mosmol $liter^{-1}$ with glucose. To simultaneously measure NLC and OHC motility, a slower sinusoidal voltage stimulus (1 Hz, 120-mV amplitude) superimposed with two higher frequency stimuli (390.6 and 781.2 Hz, 10-mV amplitude) was used (18). The intracellular solution used for testing the effect of pentanesulfonate on NLC contained 150 mM 1-pentanesulfonate, 0.5 mM CsCl, 1 mM EGTA, and 10 mM HEPES (pH 7.3). The intracellular and extracellular solutions used for testing the effect of iodide on NLC and OHC motility were identical and contained 134 mM CsI, 6 mM CsCl, 10 mM EGTA, 2 mM $MgCl_2$, and 10 mM HEPES (pH 7.3). When recording with iodide, the silver electrodes were iodinated with concentrated CsI. Intracellular pressure was kept at 0 mm Hg, and current data were collected by jClamp (SciSoft Co., New Haven, CT) using a fast Fourier transform-based admittance analysis to determine NLC (19). OHC electromotility was captured using a WV-CD22 digital camera (Panasonic, Japan), and ImageJ was used to analyze sequential images as described previously (18).

Generation of Prestin Mutants and Evaluation of NLC in HEK293T Cells—The mutated prestin constructs (shown in Fig. 4) were cloned into a pEGFP-N2 vector as described previously (16). HEK293T cells were then transfected with the mutated prestin-expressing plasmids, and NLC was measured as described previously (20).

NLC and Motility Data Analyses—In this study, we describe the voltage-dependent charge movement (q) and the resulting electromotility (d) of prestin by using the two-state Boltzmann model. Charge movement (q) is described by Equation 1.

$$q = \frac{Q_{\max}\exp[\alpha(V_m - V_{pk})]}{1 + \exp[\alpha(V_m - V_{pk})]} + C_{lin}V_m \qquad \text{(Eq. 1)}$$

Q_{max} is the maximum charge transfer, and α ($=z_{app}e/k_BT$) is the slope factor of the voltage-dependence of charge transfer where z_{app} is apparent valence of charge, e is electron charge, k_B is the Boltzmann constant, and T is absolute temperature. V_m is the membrane potential, and V_{pk} is the voltage at which the maximum charge movement per voltage is attained. Similarly, the voltage-dependent cell length change is described by Equation 2.

$$d = \frac{d_{\max}\exp[\alpha(V_m - V_{pk})]}{1 + \exp[\alpha(V_m - V_{pk})]} + d_0 \qquad \text{(Eq. 2)}$$

d_{max} is the maximum cell length change, and d_0 is the minimum length of OHCs at infinitely depolarized membrane potentials. Differentiation of Equation 1 in terms of V_m yields Equation 3 for membrane capacitance (C_m).

$$C_m = \frac{\alpha Q_{\max}\exp[\alpha(V_m - V_{pk})]}{\{1 + \exp[\alpha(V_m - V_{pk})]\}^2} + C_{lin} \qquad \text{(Eq. 3)}$$

In cases where prestin-dependent changes in the specific membrane capacitance (ΔC) are evident, the following equation was used to analyze NLC.

$$C_m = \frac{\alpha Q_{\max}\exp[\alpha(V_m - V_{pk})]}{\{1 + \exp[\alpha(V_m - V_{pk})]\}^2} + \frac{\Delta C}{1 + \exp[\alpha(V_m - V_{pk})]} + C_0 \qquad \text{(Eq. 4)}$$

C_0 represents linear capacitance, and ΔC represents the combination of prestin-dependent changes in membrane area and in either the dielectric constant or thickness of the cell membrane (18, 21). To explain NLC for OHCs derived from 499-prestin heterozygous mice (499het), the following monomer (Equation 5), dimer (Equation 6), trimer (Equation 7), and tetramer (Equation 8) binomial distribution models were used for curve fit analyses. $C_{m(WT)}$ and $C_{m(499ki)}$ were fixed using the experimentally obtained NLC parameters summarized in Table 1. The expression ratio of wild-type (WT-) and 499-prestin in 499het OHCs was defined as r:$(1 - r)$ for each model.

$$C_{m(499het)} = rC_{m(WT)} + (1 - r)C_{m(499ki)} \qquad \text{(Eq. 5)}$$

$$C_{m(499\text{het})} = r^2C_{m(\text{WT})} + 2r(1-r)C_{m(\text{WT}/499)} + (1-r)^2C_{m(499\text{ki})} \quad \text{(Eq. 6)}$$

$$C_{m(499\text{het})} = r^3C_{m(\text{WT})} + 3r^2(1-r)C_{m(\text{WT}^2/499)} + 3r(1-r)^2C_{m(\text{WT}/499^2)} + (1-r)^3C_{m(499\text{ki})} \quad \text{(Eq. 7)}$$

$$C_{m(499\text{het})} = r^4C_{m(\text{WT})} + 4r^3(1-r)C_{m(\text{WT}^3/499)} + 6r^2(1-r)^2C_{m(\text{WT}^2/499^2)} + 4r(1-r)^3C_{m(\text{WT}/499^3)} + (1-r)^4C_{m(499\text{ki})} \quad \text{(Eq. 8)}$$

Model Comparisons (Corrected Akaike Information Criterion)—For comparing the models (Equations 5–8), the F-test cannot be used because the models are not mathematically nested to each other. Therefore, Akaike's method (corrected Akaike Information Criterion (AICc)) was used for the comparisons (18, 22), and AICc scores were calculated using Equation 9,

$$\text{AICc} = N\ln\frac{SS}{N} + 2K + \frac{2K(K+1)}{N-K-1} \quad \text{(Eq. 9)}$$

where N is the number of data points used for a curve-fit analysis, SS is the absolute sum of squared difference, K is the number of free-fitting parameters plus one. A model with the lowest AICc score is generally accepted as the most likely to correctly represent the data. Prism (GraphPad Software) was used for the curve-fitting analysis of both motility and NLC.

Co-immunoprecipitation Assay—Baculovirus expressing WT-prestin tagged with an N-terminal FLAG epitope and C-terminal GFP and baculovirus expressing 499-prestin tagged with a C-terminal myc epitope were generated according to the manufacturer's instructions (Invitrogen). Approximately 2×10^7 sf9 cells were infected either singly or doubly with the baculovirus and cultured for 2 days at 28 °C. The infected cells were collected and washed with a buffer containing 150 mM NaCl, 30 mM Tris-Cl, and 5 mM EGTA (pH 7.5). Cells were lysed by sonication on ice in a buffer containing 150 mM NaCl, 30 mM Tris-Cl, 0.2 mM EGTA, 0.1 mM β-mercaptoethanol, and 20 mM n-dodecyl β-maltoside (pH 7.5) supplemented with 50 μg/ml leupeptin. Soluble and insoluble fractions were separated by centrifugation (18,000 $\times$ g for 30 min at 4 °C) and applied to an anti-FLAG M2-agarose column (Sigma). The column was washed with a 5-column volume of a buffer containing 150 mM NaCl, 30 mM Tris-Cl, 0.2 mM EGTA, and 10 mM n-dodecyl β-maltoside (pH 7.5). Bound protein was eluted using a glycine buffer containing 2 mM n-dodecyl β-maltoside (pH 3.5) and analyzed by Western blot using anti-FLAG (OctA-Probe D-8, Santa Cruz Biotechnology) and HRP-conjugated anti-myc (46-0709, Invitrogen). The co-immunoprecipitation assay was repeated three times to confirm reproducibility.

Bioinformatics—Over 200 non-redundant sequences of prestin and other SLC26 members were obtained by PSI-BLAST search and aligned using Clustal Omega to generate sequence logos by WebLogo (23).

RESULTS

Motor Characteristics of 499-prestin—Prestin-dependent charge movement is manifest in the bell-shaped, voltage-dependent membrane capacitance referred to as NLC (24, 25).

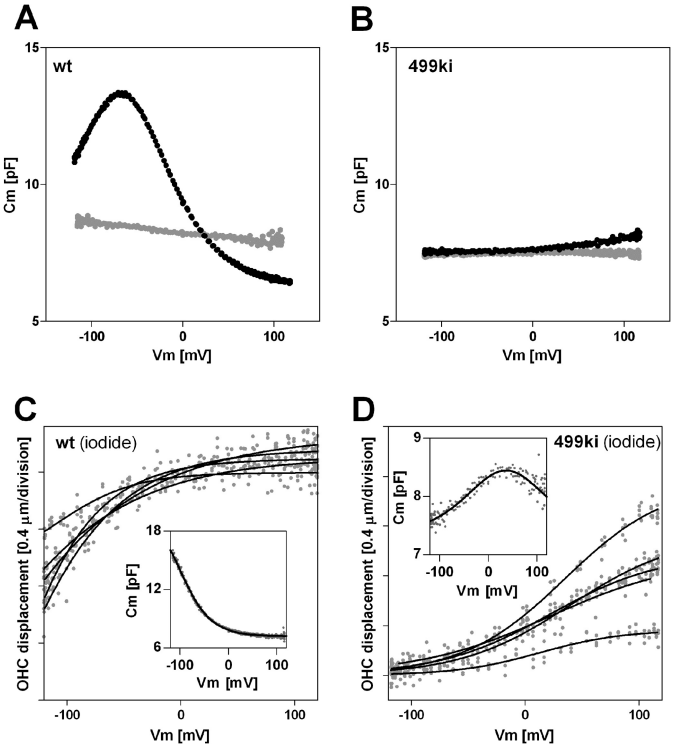

FIGURE 1. **499-prestin is a functional motor.** *A* and *B*, effect of pentanesulfonate on WT (*A*) and 499ki OHCs (*B*). NLC was measured in the presence (*gray*) or absence (*black*) of pentanesulfonate. *C* and *D*, motor function of WT (*C*) and 499ki OHCs (*D*) measured in the presence of iodide. Five representative results of OHC displacement are shown together with a representative NLC (*inset*). Typical voltage-dependent OHC displacement and bell-shaped NLC of 499ki became evident due to the hyperpolarizing V_{pk} shift induced by iodide. The motility responses were analyzed using Equation 2 (*solid lines*).

OHCs derived from WT mice display typical NLC profiles (Fig. 1*A*, *black*). In contrast, OHCs derived from 499-prestin knockin (499ki) mice show very small NLC within the ±120-mV observation window because of the extremely depolarized voltage operating point (V_{pk}) of 499-prestin under normal recording conditions using intracellular chloride (Fig. 1*B*, *black*; also see Fig. 6*A*) (5). To confirm the authenticity of motor function, we measured the NLC of 499ki OHCs in the absence of chloride by using a pentanesulfonate solution, which is known to attenuate the magnitude of the NLC peak by reducing α (Fig. 1*A*, *gray*) (6, 26). The NLC of 499-prestin observed at depolarizing voltages was almost completely flattened by pentanesulfonate (Fig. 1*B*, *gray*), suggesting that the rising C_m observed at positive V_m does indeed represent 499-prestin activity. We also measured NLC and electromotility of WT and 499ki OHCs in the presence of iodide (Fig. 1, *C* and *D*). For WT-prestin, iodide is known to shift V_{pk} in the hyperpolarizing direction (26). The bell-shaped NLC (Fig. 1*D*, *inset*) and displacement of 499ki OHCs (Fig. 1*D*) became evident with iodide, confirming that 499-prestin is functional as a motor albeit with altered properties. The OHC displacement observed in 499ki OHCs with iodide is quite large (~1 μm) compared with the relatively small charge movement (201 ± 38 fC; Fig. 1*D*, *inset*), implying that 499-prestin induces a greater displacement for a given charge movement compared with WT-prestin. However, because OHC displacement was measured using a 1-Hz voltage stimulus, whereas the associated NLC was measured using two

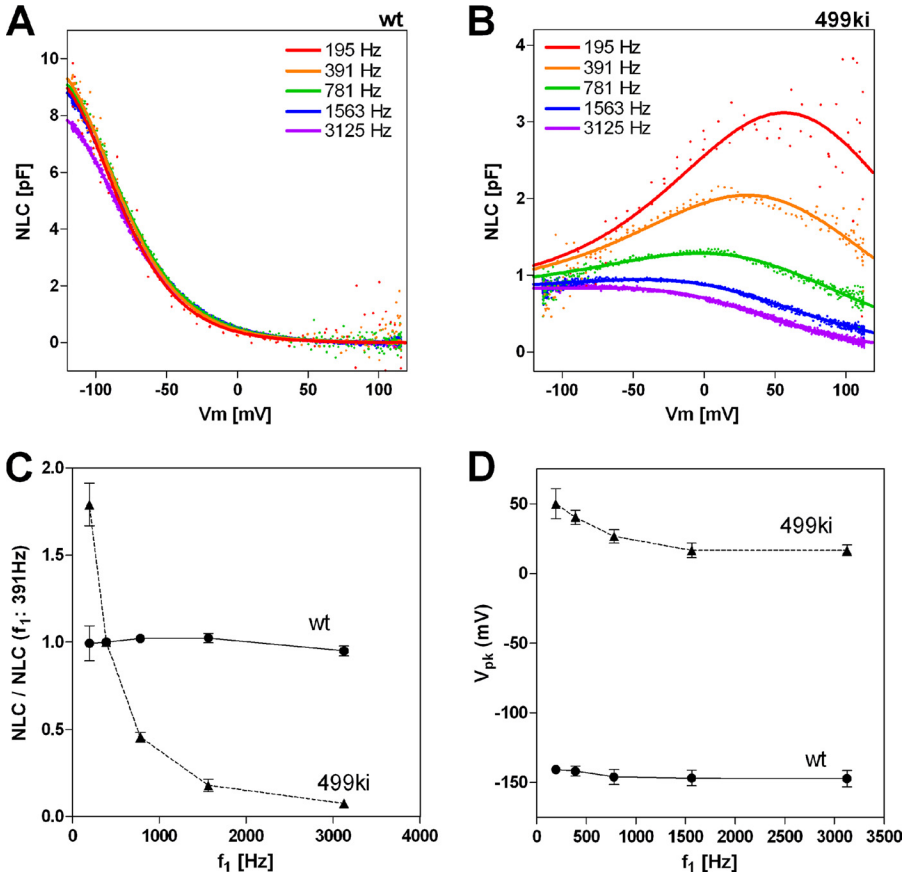

FIGURE 2. **Voltage stimulus frequency-dependent NLC measurement.** Examples of stimulus frequency-dependent NLC measurements on WT (*A*; $n = 5$) and 499ki OHCs (*B*; $n = 5$) are shown. NLC measurements were performed using five different f_1 frequencies with corresponding f_2 frequencies being twice as large as f_1. Equations 3 and 4 were used to determine the Q_{max} values of WT and 499ki OHCs, respectively. The obtained Q_{max} values were divided by those determined at 390.6 Hz, and resulting quotients were plotted as a function of the f_1 stimulus frequency in *C*. V_{pk} values were also plotted as a function of the f_1 stimulus frequency in *D*. *Error bars* represent S.D.

small sinusoidal voltage stimuli at higher frequencies ($f_1 = 391$ Hz, $f_2 = 781$ Hz) superimposed onto the 1-Hz stimulus (see "Experimental Procedures"), the relatively small charge displacement seen in 499ki OHCs could result from reduction in motor kinetics, which may be induced by the V499G/Y501H mutation. In other words, the stimulus frequencies used for measuring NLC in 499-prestin (391 and 781 Hz) might be too high to induce charge displacements that are comparable with WT-prestin. To test this possibility, we performed stimulus frequency-dependent NLC measurements on 499ki OHCs under the iodide condition. The measurements were also performed on WT OHCs under the same iodide condition for comparison (Fig. 2, *A* and *B*) and with chloride (for WT; supplemental Fig. S1). To quantitatively describe the frequency dependence of NLC, we divided the magnitude of NLC (Q_{max}) by that determined at $f_1 = 391$ Hz (Fig. 2*C*). We used recordings at 391 Hz (f_1) as reference because it is our standard stimulus condition used for most NLC recordings. As expected, the magnitudes of NLC of WT OHCs did not decrease significantly as the stimulus frequency increased ($f_1 = 195–3125$ Hz; $f_2 = 2f_1 = 391–6250$ Hz), reaffirming the excessively fast motor kinetics of WT-prestin (Fig. 2, *A* and *C*) (10). In contrast, the NLC of 499ki OHCs showed significant frequency dependence (Fig. 2, *B* and *C*), suggesting that the motor kinetics of 499-prestin is in fact significantly impaired by V499G/Y501H mutation. Because the frequency-dependent NLC of 499ki plateaued at higher frequencies, which do not limit the admittance analysis-based capacitance measurement due to sufficiently large stimulus pipette conductance (~0.1 microsiemen), it is likely that the small and apparently widened NLC of 499ki seen at higher frequencies (Fig. 2*B*) is controlled by the static conformation (compacted *versus* elongated)-dependent change in the specific capacitance of the cell membrane (21). Therefore, Equation 4 was used to analyze the NLC of 499ki OHCs. Calculations indicate that the magnitude of ΔC, which represents incremental capacitance due to the prestin-dependent change in membrane area plus any change in membrane thickness, was determined to be 0.74 ± 0.07 pF (mean ± S.D., $n = 5$). Inclusion of the ΔC term (fixed at 0.74 pF) did not significantly change the stimulus frequency-dependent NLC profile of WT OHCs due to its relatively smaller contribution (data not shown). A hyperpolarizing shift of V_{pk} at higher stimulus frequencies was also evident in 499ki (Fig. 2*D*). Such stimulus frequency-dependent V_{pk} shift was not evident in WT. The reason for the shift seen in 499ki is unclear. Because the overall circuit admittance is significantly limited by the membrane plus stimulus pipette conductances, *i.e.* not by the prestin-related capacitance change at lower stimulus frequencies, we could not determine the maximum charge displacement of 499ki. However, our NLC measurements allow us to predict the magnitude of NLC that should correspond to

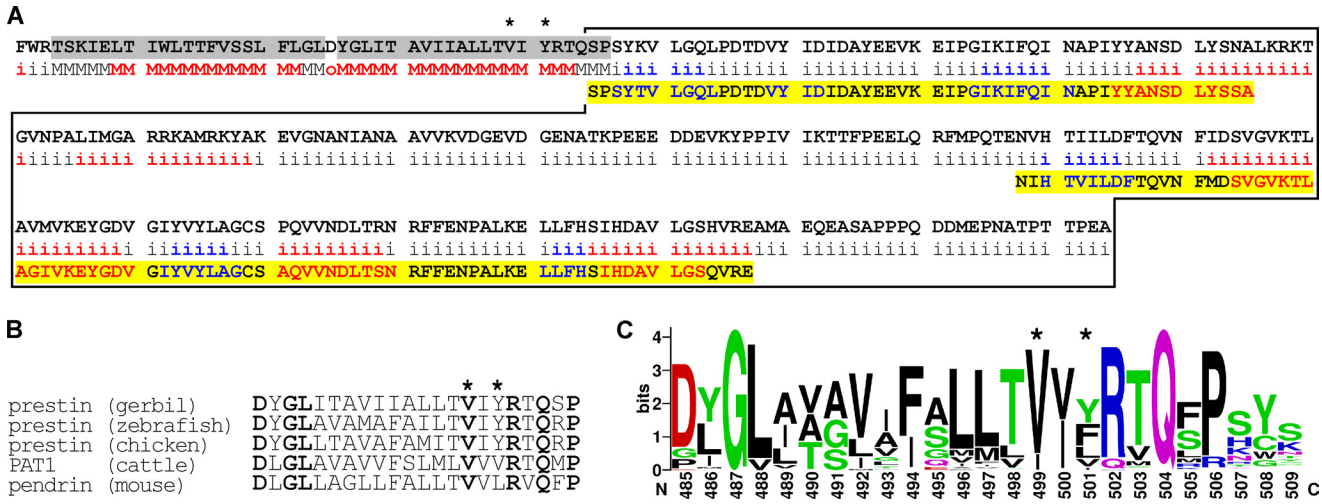

FIGURE 3. **Val-499/Tyr-501 site of prestin.** *A*, predicted locations of transmembrane segments and secondary structures. Only a partial sequence of gerbil prestin (461–744) including the intracellular C-terminal domain (enclosed by the *black lines*) is shown. The locations of Val-499 and Tyr-501 are indicated by *asterisks*. Shaded in *gray* are membrane-spanning regions associated with the 11th and 12th transmembrane domains of prestin predicted by the SCAMPI-msa algorithm. Regions projected to be intracellular, membrane-spanning, or extracellular are noted as "*i*," "*M*," and "*o*," respectively. A secondary protein structure prediction server, Jpred3, was also used to predict α-helix (*red*) and β-sheet (*blue*) regions. Partial amino acid sequences in the C-terminal domain of rat prestin whose tertiary structures are solved (27) are also shown below the corresponding sequence of gerbil prestin (shaded in *yellow*). *B*, comparison of the amino acid sequence at the Val-499/Tyr-501 site in various species. A partial amino acid sequence of gerbil prestin (485–506) along with the corresponding sequences of other SLC26A family members from different organisms is shown. The locations of Val-499 and Tyr-501 are indicated by *asterisks*. The *bold characters* indicate amino acids that are conserved among the five SLC26A proteins shown. *C*, a graphical representation of amino acid residue conservation at the Val-499/Tyr-501 site. The locations of Val-499 and Tyr-501 are indicated by *asterisks*. Amino acids are colored according to their chemical properties: *green* for polar (Gly, Ser, Thr, Tyr, Cys, Gln, and Asn), *blue* for basic (Lys, Arg, and His), *red* for acidic (Asp and Glu), and *black* for hydrophobic (Ala, Val, Leu, Ile, Pro, Trp, Phe, and Met) amino acids. The relative *height* of any given *logo/letter* represents the frequency of that amino acid, whereas the total *height* of the *stack* represents the degree of sequence conservation (maximum, 4.3 bits).

the motility data measured at 1 Hz. The data indicate that the NLC would be at least twice that determined at 391 Hz (Fig. 1*D*). This estimate implies that the fundamental motor mechanism of prestin, besides its slowed kinetics, would probably not be significantly affected by the V499G/Y501H mutation.

The Val-499/Tyr-501 Site—To gain insights into the structural-functional relationships that underlie the fast motor kinetics of prestin, we performed a bioinformatics analysis using the primary sequence of gerbil prestin because the structure of prestin, except for a portion of its C-terminal domain (27) and its membrane topology, have not been defined. Fortunately, the membrane topology of the bacterial member of the SulP/SLC26 family, BicA, was predicted using the SCAMPI-msa algorithm, and this result agrees with the membrane topology of this protein determined experimentally (28). Because prestin also belongs to the SLC26 family, we ran the SCAMPI-msa algorithm hoping to obtain a better prediction of the membrane topology of prestin. As shown in Fig. 3*A*, the algorithm predicted the Val-499/Tyr-501 site (indicated by "*") to lie within the C-terminal end of the 12th transmembrane segment (shaded in *gray*) that immediately precedes the C-terminal domain (enclosed by *black lines*). In addition, locations of α-helixes (shown in *red*) and β-strands (shown in *blue*) were predicted by JPred3, and these predictions of the secondary structure of gerbil prestin agree with those solved experimentally for rat (27, 28) (shaded in *yellow* with the same color coding). The predictions made by these two independent programs are consistent with each other; *i.e.* the locations of transmembrane segments predicted by SCAMPI-msa (shaded in *gray*) overlap with the locations of α-helixes predicted by JPred3 (shown in *red*). These predictions are also similar to the published location of Val-499/Tyr-501 (5).

The degree of residue conservation for the Val-499/Tyr-501 region was also interrogated using a PSI-BLAST search followed by multiple sequence alignment. Fig. 3*B* provides five partial sequences of SLC26 proteins containing the Val-499/Tyr-501 site. Among these, only gerbil prestin is electromotile. There seems to be no obvious correlation between residue conservation at the 499 and 501 positions and function, *i.e.* motor *versus* transporter. However, the high degree of residue conservation at the 499 position (Fig. 3*C*) suggests the importance of this site for fundamental properties shared among SLC26 proteins. Compared with 499, the 501 position is less conserved. At the very least, the presence of Tyr at the 501 position does not seem to correlate with the voltage-dependent motor activity, which is only observed in mammalian and platypus prestins. The results of this exercise indicate that there seems to be nothing obviously special about 499 and 501 that would induce one to mutate them to learn something about the molecular mechanisms underlying the motor action of prestin, hence the serendipitous nature of this discovery (16).

Motor Properties of Various Single/Double Mutations of Amino Acids 499 and 501—To gain further insight into the unique motor properties conferred by the V499G/Y501H mutation, we generated a series of prestin mutants that were heterologously expressed in HEK293T cells and measured NLC to examine how charge translocation is affected (Fig. 4). The α value is a useful metric for evaluating these mutations and comparing the results among different prestin constructs. Recall that α is determined by both valence (z) and distance (δ) of

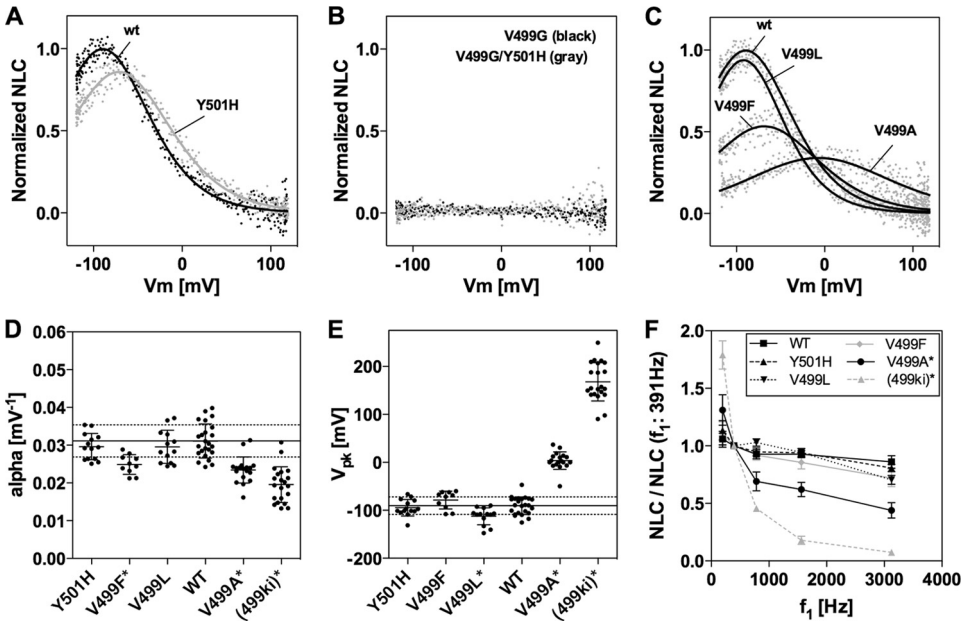

FIGURE 4. **NLC of various prestin constructs measured in HEK293T cells.** *A*, examples of NLC measured on HEK293T cells expressing WT-prestin or Y501H prestin. *B*, examples of NLC measured on HEK293T cells expressing V499G or V499G/Y501H prestin. Each construct contains a C-terminally attached enhanced GFP tag for visual confirmation of successful heterologous expression. *C*, NLC of various prestin mutants. Representative NLC of WT-prestin and V499L, V499F, and V499A prestin mutants are shown. *D* and *E*, summary of NLC parameters in various prestin mutants. All NLC measurements were performed under the chloride condition. NLC data were analyzed using Equation 3 and Equation 4 (for V499A) to determine NLC parameters for each prestin construct. Obtained α and V_{pk} values are summarized in *D* and in *E*, respectively. The α and V_{pk} values (mean $\pm$ S.D.) were as follows: WT, 0.031 $\pm$ 0.005 mV^{-1} and -91 ± 18 mV ($n = 24$); Y501H, 0.030 $\pm$ 0.003 mV^{-1} and -95 ± 17 mV ($n = 14$); V499A, 0.023 $\pm$ 0.003 mV^{-1} and 3.5 $\pm$ 18 mV ($n = 18$); V499L, 0.030 $\pm$ 0.004 mV^{-1} and -113 ± 18 mV ($n = 13$); and V499F, 0.025 $\pm$ 0.003 mV^{-1} and -79 ± 19 mV ($n = 10$). The *horizontal solid* and *broken lines* indicate the means and S.D. of WT. The *asterisks* shown after the construct name indicate a statistically significant difference ($p < 0.05$) compared with WT. Because the NLC of V499G and V499G/Y501H was too small to be detected in HEK293T cells, the α and V_{pk} data for V499G/Y501H were obtained from 499ki OHC recordings (Table 1 and Fig. 6). *F*, voltage stimulus frequency dependence. NLC measurements were performed on HEK293T cells expressing various prestin constructs (WT ($n = 6$), Y501H ($n = 5$), V499L ($n = 5$), V499F ($n = 4$), and V499A ($n = 7$)) and using five different f_1 frequencies (195.3, 390.6, 781.3, 1563, and 3125 Hz). The corresponding f_2 frequencies were twice as large as f_1. The obtained Q_{max} values were divided by those determined at 390.6 Hz, and resulting quotients were plotted against the f_1 stimulus frequency. The data for *(499ki)* are from Fig. 2. Examples of stimulus frequency-dependent NLC can be found in supplemental Fig. S3. *Error bars* represent S.D.

voltage-induced charge movement within the prestin molecule ("z_{app}" defined in Equations 1–3 is an apparent valence that is written as $z\delta$) whose magnitude could reflect the kinetics of voltage-induced charge displacement. Voltage-induced charging/discharging a capacitor is a fast process, and the phase is 90° advanced relative to that of the voltage stimulus. NLC is determined from the magnitude of this phase-shifted current component (19). If stimulus frequency exceeded the motor kinetics of prestin, underestimation of prestin-related charge movement would occur. In the two-state Boltzmann model, this would manifest as reduction in α, and reduction in Q_{max} should accompany this reduction in α because Q_{max} is defined as $\alpha N k_B T$ where N is the number of prestin molecules (18). In fact, reductions in α associated with decreases in Q_{max} at higher stimulus frequencies can be observed in WT OHCs (supplemental Fig. S1).

We first tested V499G and Y501H prestins so that the effect of each individual mutation was evaluated separately. Y501H prestin showed WT-like NLC (Fig. 4*A*) with similar α, V_{pk}, and kinetics (Fig. 4, *D–F*). Because NLC of V499G was too small to be confidently analyzed in HEK293T cells as was the case for V499G/Y501H (Fig. 4*B*), the NLC of 499ki OHCs measured under the chloride condition was used for comparison in Fig. 4, *D* and *E*, and indicated as "*(499ki)*." For the same reason, the degree of stimulus frequency-dependent reduction in Q_{max} determined for 499ki OHCs under the iodide condition (Fig. 2) was used in Fig. 4*F* for comparison (also indicated as *(499ki)*). A significant reduction in α, shift in V_{pk}, and reduction in the degree of stimulus frequency-dependent Q_{max} are evident in 499ki, and similar changes are assumed for V499G. The absence of detectable NLC (Fig. 4*B*) is not due to misfolding and/or mistargeting of the prestin mutants expressed in HEK293T cells because stimulus frequency-dependent NLC of those mutants determined under the iodide condition (supplemental Fig. S2) qualitatively resembles that of 499ki OHCs measured under the same condition as in Fig. 2*B*. These observations suggest that the unique motor property found in V499G/Y501H prestin is attributable to V499G. This conclusion is consistent with the fact that the 501 site is not highly conserved among SLC26 family members as noted above, indicating that it is probably not important for function, be it transport or electromotility.

We then generated additional prestin mutants focusing on the 499 site (Fig. 4*C*). Because Val or Ile dominates the 499 position (Fig. 3*C*), a hydrophobic residue of a certain size appears to be required, and both of these properties are significantly altered in V499G. In fact, replacement with Leu did not significantly change α or the fast motor kinetics (Fig. 4, *D* and *F*), consistent with the fact that Leu is similar in size and hydrophobicity to Ile. V_{pk} of V499L, however, showed a hyperpolarizing shift (Fig. 4*E*), suggesting the importance of the 499 site for determining the voltage operating point of prestin. We then

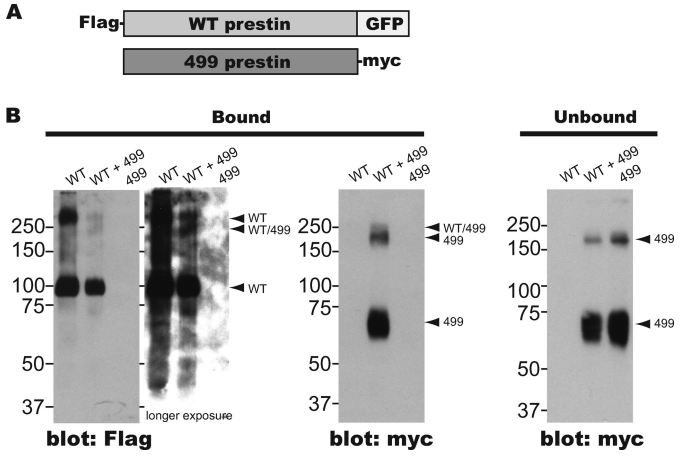

FIGURE 5. **Heteromer formation between WT- and 499-prestin.** *A*, WT- and 499-prestin constructs used for the copurification assay. Wild-type prestin was tagged with an N-terminal FLAG epitope and C-terminal GFP, whereas the 499-prestin construct was tagged with a C-terminal myc epitope. *B*, copurification of 499-prestin with WT-prestin. The prestin constructs shown in *A* were singly or coexpressed in sf9 cells, purified using a FLAG affinity column, and analyzed by Western blot. The *numbers* indicate molecular masses in kDa.

replaced Val with Phe to further examine the steric effect of an amino acid residue at the 499 site without altering the degree of hydrophobicity. The V499F mutation resulted in significant decrease in α (Fig. 4*D*). Although the reduction in α seems to be qualitatively manifest in the relatively greater degree of reduction of NLC at higher stimulus frequencies compared with WT, Y501H, and V499L (Fig. 4*F*), the difference was statistically indistinguishable from that of WT. Unlike V499L, V499F did not show significant shifts in V_{pk} (Fig. 4*E*). These results suggest that the hydrophobicity of the residue at the 499 site is more important than molecular size for defining the motor characteristics of prestin. We also replaced Val with another nonpolar residue, Ala, whose hydrophobicity is intermediate between Val and Gly. As expected, NLC phenotypes were intermediate between WT-prestin and 499-prestin in terms of α, V_{pk}, and the kinetics (Fig. 4, *D–F*). These results may imply that hydrophobicity at the 499 site is important for the stability of the last transmembrane helix in the membrane and that this structural integrity is required to support fast voltage-dependent motor function.

Heteromer Formation between WT-prestin and 499-prestin—Prestin is known to form multimers that could conceivably function as minimal motor units (11–15). It is also known that 499-prestin forms multimers just like WT-prestin (5). Because this self-association may be essential for the energy transduction mechanism of prestin, the drastic alteration in motor properties seen in 499-prestin may indicate a change in the way prestin subunits interact. If this were the case, 499-prestin subunits might not be readily interchangeable with WT-prestin. To test this idea, we examined heteromer formation between WT- and 499-prestin in a baculovirus/sf9 heterologous expression system, which attains a high efficacy of coexpression in sf9 cells that are known to produce functional prestin (29). Epitope-tagged prestin constructs were used because antibodies that distinguish 499- from WT-prestin are not available. FLAG-tagged WT-prestin and myc-tagged 499-prestin constructs were used for testing heteromer formation. Use of GFP (~27 kDa)-tagged WT-prestin allows the various constructs to be identified by differences in molecular mass (Fig. 5*A*). The WT-prestin (FLAG-WT-prestin-GFP, ~110 kDa) and/or the 499-prestin (499-prestin-myc, ~82 kDa) were expressed in sf9 cells and purified with a FLAG affinity column. As expected, the WT-prestin construct bound to the FLAG affinity column irrespective of the expression of the 499-prestin construct. In contrast, 499-prestin did not bind to the column by itself when singly expressed but did bind to the column when coexpressed with WT-prestin (Fig. 5*B*, *left*). Absence of the bound 499-prestin band was not due to reduced protein expression because protein was clearly detected in the unbound fraction (Fig. 5*B*, *right*). Dimeric bands that were observed for WT- and 499-prestins extracted from WT and 499ki OHCs (5) were also evident for constructs expressed in sf9 cells especially when longer exposures were used. The fact that 499/499 multimers are collected by the FLAG column is indicative of trimer/tetramer formation between WT- and 499-prestin. Additional bands with molecular masses slightly different from those of a WT-prestin homodimer and a 499-prestin homodimer due to the addition of GFP to the WT-prestin construct were also seen (labeled as "WT/499"; Fig. 5*B*). The greater reactivity of the 499 multimer band *versus* the WT/499 band probably reflects the greater number of myc epitopes associated with 499 homomultimers when compared with WT/499 heteromultimers. Collectively, these results suggest that WT- and 499-prestin form homomultimers in a similar fashion.

It is likely that WT-/499-prestin heteromers exhibit unique motor properties that would manifest in a distinct NLC, providing indirect evidence for WT-/499-prestin heteromer formation. To test this prediction, we crossed WT and 499ki mice to obtain 499-prestin heterozygous (499het) mice and measured NLC of OHCs isolated from these mice in which both WT- and 499-prestins are expressed. Because prestin expression density in OHCs is ~10 times higher than that typically achieved in mammalian and insect cell lines, it is possible to examine NLC with higher resolution and to define contributions originating from multiple prestin components. Results from 499het OHCs were compared with WT and 499ki OHCs measured under the same conditions (chloride, 391/781 Hz) (Fig. 6). Equation 3 was successful for interpreting the NLC data obtained in 499het OHCs, and the resulting NLC parameters for OHCs harvested from all three genotypes are summarized in Fig. 6, *B–E*, and in Table 1. The α (Fig. 6*B*) and V_{pk} (Fig. 6*C*) values of 499het were statistically distinct from those of WT, supporting the biochemical evidence showing formation of WT-/499-prestin heteromers (Fig. 5). The C_{lin} values were similar among WT, 499het, and 499ki, suggesting that the total number of prestin molecules expressed is similar among WT, 499het, and 499ki (Fig. 6*D*). In addition, charge densities of 499het OHCs were similar from cell to cell (Fig. 6*E*), indicating that the expression ratio of WT- and 499-prestin is constant among 499het OHCs. Stimulus frequency dependence of 499het was very similar to that of WT (Fig. 6, *F–H*), strongly suggesting that the fast motor kinetics of WT-prestin and the slowed motor kinetics of 499-prestin remain unaffected within WT-/499-prestin heteromers. This independence of the motor kinetics allowed us to predict that the contribution of voltage-

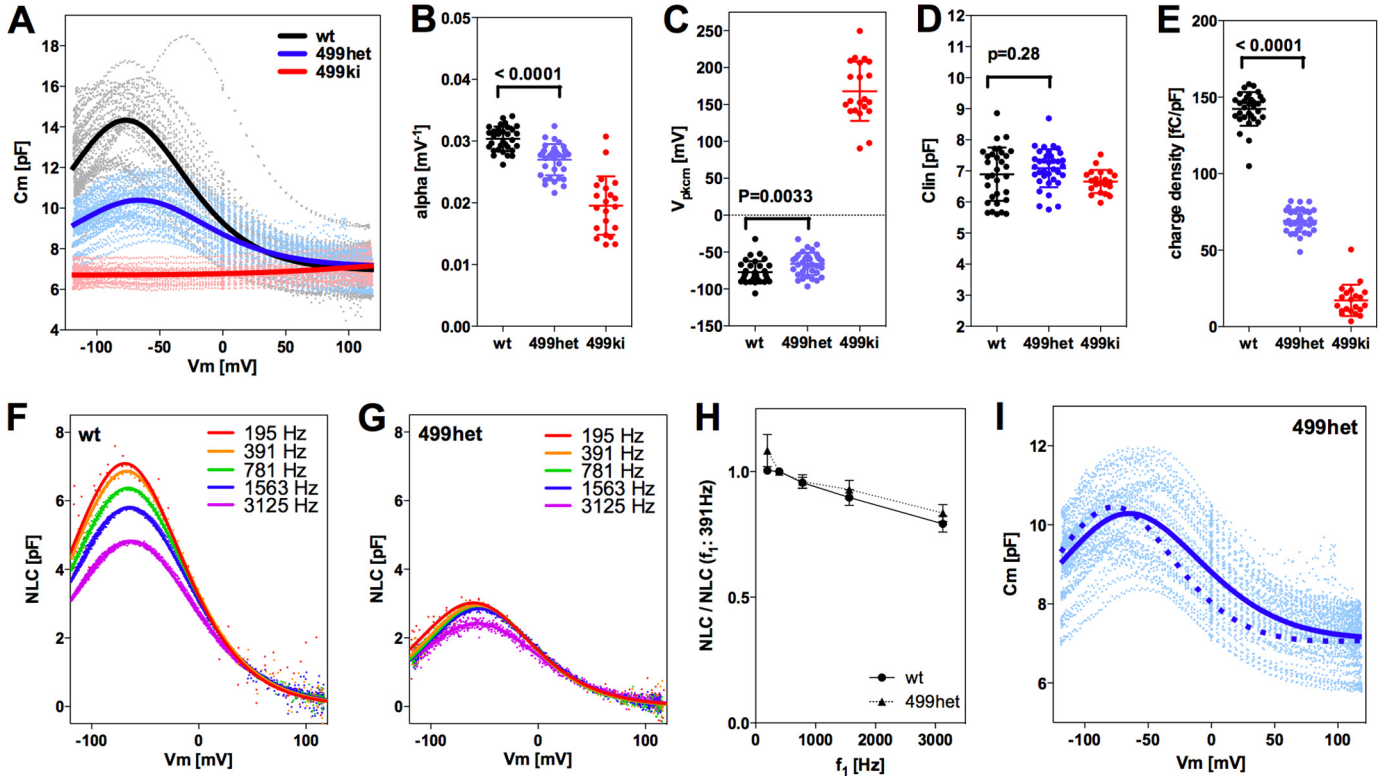

FIGURE 6. **Distinct prestin-dependent charge movement of 499het.** *A–E*, NLC observed in WT, 499het, and 499ki OHCs. *Gray*, *blue*, and *red dots* represent individual NLC recordings. Curve fit analyses using Equation 3 were performed on individual recordings to obtain the statistics summarized in *B–E* and Table 1 as means ± S.D. Average NLC curves generated using the NLC parameters summarized in Table 1 are shown with *bold solid lines* in *A*. *F–H*, voltage stimulus frequency-dependent NLC in WT and 499het OHCs. NLC measurements were performed on WT ($n = 3$) and 499het ($n = 4$) OHCs under the chloride condition using five different f_1 frequencies (195.3, 390.6, 781.3, 1563, and 3125 Hz). The corresponding f_2 frequencies were twice as large as f_1. Representative recordings for WT (*F*) and 499het (*G*) are shown. The obtained Q_{max} values were divided by those determined at 390.6 Hz, and resulting quotients were plotted against f_1 stimulus frequency in *H*. Differences between WT and 499het are not significant. *I*, interpretation of 499het NLC. Using WT NLC ($C_{m(WT)}$) and 499ki NLC ($C_{m(499ki)}$) as defined by the NLC parameters summarized in Table 1 (shown with *bold black* and *red lines* in *A*), four different prestin models (monomer (Equation 5), dimer (Equation 6), trimer (Equation 7), and tetramer (Equation 8)) were tested to see which model best explains the observed 499het NLC data shown with *pale blue dots* (total 36 NLC recordings). The *broken line* indicates the monomer-based curve fit, whereas the *solid line* indicates the dimer-based curve fit. Trimer- and tetramer-based curve fits generated lines that looked no different from that of the dimer model. Fitting parameters obtained by the analyses are summarized in Table 2. The apparent *line* at 0 mV is a result of NLC data correction by the series resistance, Rs. The NLC data were individually corrected because of different Rs values among recordings. Because the data points at 0 mV did not change with the correction, an "apparent" *vertical line* emerges. *Error bars* represent S.D.

TABLE 1

Summary of the NLC parameters of WT, 499het, and 499ki OHCs determined in Fig. 6A

Data represent average ± S.D.

	WT ($n = 32$)	499het ($n = 36$)	499ki ($n = 21$)
α (mV^{-1})	0.030 ± 0.002	0.027 ± 0.003	0.020 ± 0.005
V_{pk} (mV)	−77 ± 15	−66 ± 15	168 ± 40
Q_{max} (fC)	979 ± 129	490 ± 57	115 ± 73
C_{lin} (pF)	6.9 ± 0.9	7.1 ± 0.6	6.7 ± 0.4
Charge density (fC/pF)	142 ± 11	69 ± 7.4	17 ± 10

induced charge movement of 499-prestin to the overall NLC of 499het is very small compared with that of WT-prestin under our experimental conditions (391/781 Hz). Therefore, the observation that charge density of 499het was approximately half of WT (Fig. 6*E*) strongly implies that the expression ratio of WT- and 499-prestin in 499het OHCs is approximately equal.

We also performed further analyses on 499het NLC because there should be individual NLC components derived from WT-prestin and 499-prestin even if WT-/499-prestin heteromers with distinct NLC parameters were not present. Therefore, curve fit analyses were performed on the 499het NLC data based on monomer (Equation 5), dimer (Equation 6), trimer (Equation 7), and tetramer models (Equation 8) by defining the NLC parameters of WT-prestin monomer or homomers ($C_{m(WT)}$) and 499-prestin monomer or homomers ($C_{m(499ki)}$) using parameters summarized in Table 1 for WT and 499ki (Fig. 6*I*). The expression ratio of WT- and 499-prestin in 499het OHCs was defined as r:$(1 - r)$ for each model. NLC parameters (α, V_{pk}, Q_{max}, and C_{lin}) of the WT-/499-prestin heteromers were set as free fitting parameters for the oligomer models (Equations 6–8). The curve fit results are summarized in Tables 2 and 3. A significant improvement in curve fit by the dimer model (Fig. 6*I*, *solid line*) compared with the monomer model (Fig. 6*I*, *broken line*) is clearly manifest in the lower sum of squares and the resulting higher R^2 values (Table 3). Further improvements using trimer and tetramer models were not obvious. The likelihood of each model being correct compared with the other models was evaluated by calculating AICc scores

TABLE 2

Summary of fitting parameters determined in Fig. 6I based on different prestin models

	monomer	dimer	trimer		tetramer		
r	0.50	0.43	0.58		0.55		
NLC		wt / 499	wt^2 / 499	wt / 499^2	wt^3 / 499	wt^2 / 499^2	wt / 499^3
α [mV^{-1}]		0.024	0.027	0.019	0.027	0.021	0.011
V_{pk} [mV]		-53	-49	-63	-59	-67	-10
Q_{max} [fC]		730	500	373	1064	270	145
C_{lin} [pF]		7.0	7.2	6.8	7.1	6.9	7.0

TABLE 3

Evaluation of four different prestin models

Parameter, the number of free-fitting parameters used for each prestin model-based curve fit analysis; SS, absolute sum of squares; R^2, goodness of fit.

	Parameter	SS	R^2	AICc
Monomer	1	4906	0.57	−1094
Dimer	5	3800	0.66	−2595
Trimer	9	3799	0.66	−2589
Tetramer	13	3799	0.66	−2581

(Equation 9). The AICc score was the lowest for the dimer model, suggesting that it is most likely to be correct. It is noted, however, that the lowest AICc score of the dimer model over trimer and tetramer models was due to the smaller number of free fitting parameters for attaining an equally good fit. Because there is experimental evidence supporting tetramer formation of prestin (11, 13, 14) and because the curve fits themselves were equally good among the oligomer models, the higher oligomer models should not be discarded solely based on this test. The expression ratio, *r*, determined by the four models ranged from 0.43 to 0.58, suggesting that approximately equal amounts of WT- and 499-prestin are present in 499het OHCs. The distinct NLC observed in 499het OHCs, which cannot be explained by simple sums of NLCs derived from WT and 499ki OHCs (Fig. 6*I*, *broken line versus solid line*), strongly supports formation of WT-/499-prestin heteromers in OHCs, which is consistent with the biochemical evidence (Fig. 5).

Functional Significance of Prestin Multimer Formation—The functional importance of prestin multimer formation is not clear. The fact that the fast motor kinetics of WT-prestin is not affected by 499-prestin in 499het OHCs (Fig. 6*H*) strongly suggests functional independence of prestin subunits in a given prestin multimer. We further examined functional independence of WT- and 499-prestin in 499het OHCs in terms of cell motility. To begin, we divided the observed OHC displacement (*d*) by the observed prestin-dependent charge movement (*q*), which was determined by the area between the NLC curve and C_{lin} within the observation window (±120 mV). This quotient was defined as the electromechanical coupling efficiency (18). Because of its very small NLC and OHC displacement observed within ±120 mV under the chloride condition, the electromechanical coupling efficiencies of 499ki OHCs were determined using iodide (Fig. 7*A*). We also determined electromechanical coupling efficiency for WT OHCs in the presence of iodide for comparison (Fig. 7*A*). Compared with WT OHCs, a significantly larger (on average 3.14-fold) electromechanical coupling was observed for 499ki OHCs under our experimental conditions (1.4 *versus* 4.4 nm/fC; Fig. 7*A*). Notice that the electromechanical coupling efficiency is defined as d/q (±120 mV) and not d_{max}/Q_{max} (±∞ mV) because this latter metric could not be

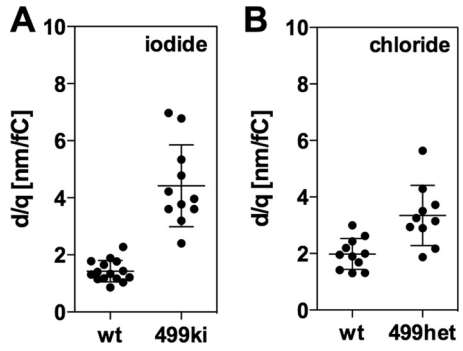

FIGURE 7. **Electromechanical coupling efficiencies of WT, 499het, and 499ki OHCs determined for the 391/781-Hz stimulus.** OHC displacements and associated NLC were measured under iodide and chloride conditions, and the resulting electromechanical coupling efficiencies were plotted in *A* and *B*, respectively. See Fig. 1 for representative recordings of WT and 499ki OHCs under iodide condition and Fig. 6 and supplemental Fig. S4 for WT and 499het OHCs under the chloride condition. The *d*/*q* values are 1.4 ± 0.4 nm/fC (average ± S.D., $n = 15$) for WT OHCs and 4.4 ± 1.4 nm/fC (average ± S.D., $n = 11$) for 499ki OHCs ($p < 0.0001$) under the iodide condition (*A*) and 2.0 ± 0.6 nm/fC (average ± S.D., $n = 11$) for WT OHCs and 3.3 ± 1.1 nm/fC (average ± S.D., $n = 10$) for 499het OHCs ($p = 0.0014$) under the chloride condition (*B*). *Error bars* represent S.D.

determined reliably for 499het OHCs expressing both WT- and 499-prestin due to the presence of multiple motor components. It is emphasized that the ~3-fold increase in electromechanical coupling efficiency is due to use of the 391/781-Hz stimulus frequency that is faster than the motor kinetics of 499-prestin. We simply used this artificially enhanced electromechanical coupling efficiency of 499ki OHCs as a metric to assess functional independence of WT- and 499-prestin in 499het OHCs.

Electromechanical coupling efficiencies of 499het OHCs were also determined under the chloride condition, and the results were compared with those of WT OHCs determined under the same condition (Fig. 7*B*). As expected, seemingly increased electromechanical coupling efficiency compared with WT was found in 499het OHCs (3.3 *versus* 2.0 nm/fC; 1.65-fold increased). We then tested the idea that the apparently increased electromechanical coupling efficiency of 499het OHCs can be explained by weighted averages of WT- and 499ki OHCs for the dimer, trimer, and tetramer models considered above (Table 2). If electromechanical coupling efficiencies of WT- and 499-prestin were assumed not to change upon heteromer formation as predicted from independence of the motor kinetics (Fig. 6*H*), then the overall electromechanical coupling efficiency of 499het for *n*-mer models could be calculated using a binomial formula,

$$\sum_{j=0}^{n} r^{n-j}(1-r)^{j}\frac{n!}{j!(n-j)!}\frac{(n-j)E_{WT}+jE_{499}}{n} \qquad \text{(Eq. 10)}$$

where r and $(1 - r)$ are the ratio of WT- and 499-prestin expressed in 499het OHCs (Equations 5–8), and E_{WT} and E_{499} are electromechanical coupling efficiencies of WT- and 499-prestin, respectively. Because the electromechanical coupling efficiency of 499het OHCs was determined by NLC/motility measurements using the ±120-mV voltage excursion, Equation 10 needs to be corrected to facilitate comparisons with the experimental observations; *i.e.* Equation 10 assumes infinite voltage excursions to capture the entire NLC profiles. Using the

values summarized in Tables 1 and 2 for each *n*-mer model, charge movement of each homomer/heteromer component that should be observed with the ±120-mV window is described by Equation 11.

$$q_j = r^{n-j}(1-r)^j Q_{\max j}\left[\frac{1}{1+\exp(-\alpha_j(+120-V_{\mathrm{pkj}}))} - \frac{1}{1+\exp(-\alpha_j(-120-V_{\mathrm{pkj}}))}\right] \quad \text{(Eq. 11)}$$

Therefore, electromechanical coupling efficiency of 499het OHCs that should be observed in the ±120-mV window (E_{obs}) is calculated as

$$E_{\mathrm{obs}} = \frac{1}{q_{T_{j=0}}}\sum_{j=0}^{n}\frac{n!q_j}{j!(n-j)!}\frac{(n-j)E_{\mathrm{WT}}+jE_{499}}{n} \quad \text{(Eq. 12)}$$

using Equation 13.

$$q_T = \sum_{j=0}^{n} q_j \quad \text{(Eq. 13)}$$

The relative electromechanical coupling efficiency ($E_{\mathrm{obs}}/E_{\mathrm{WT}}$) calculated for the dimer, trimer, and tetramer models using the parameters listed in Tables 1 and 2 all fall in the range of 1.6–1.7, which is comparable with the experimentally determined value of 1.65 for 499het OHCs. Note that this experimentally determined value is smaller than that predicted based on the above mentioned implication that WT- and 499-prestin function independently, *i.e.* 2.07 (computation, (1 + 3.14)/2 = 2.07). This difference occurs because the electromechanical coupling efficiency was determined by *d* and *q*, and these parameters were measured within the ±120-mV window using chloride. Hence, the motor function of 499-prestin multimers with an ~3-fold higher coupling efficiency would not be fully captured within the ±120-mV window due to their highly depolarized V_{pk}. Collectively, this exercise supports functional independence of prestin subunits in a given prestin multimer.

DISCUSSION

In the present study, we show that 499-prestin is functional as a voltage-dependent motor, although the kinetics is significantly slowed. Even at lower stimulus frequencies, motor function at physiologically relevant membrane potentials is very small due to the extreme depolarization in V_{pk}. Furthermore, our stimulus frequency-dependent NLC measurements on 499het OHCs (Fig. 6, *F–H*) together with the exercise using apparently increased electromechanical coupling efficiency of 499-prestin (Fig. 7) revealed functional independence of prestin subunits within multimer complexes. This result is consistent with a previous study proposing mechanical independence of each prestin subunit (30). However, it should be emphasized that the mechanical independence of prestin subunits needs to be discussed separately for motor kinetics and voltage-operating point (V_{pk}). Our results suggest mechanical independence of prestin subunits in connection with motor kinetics but not for the voltage-operating point. Notice that the observed V_{pk} of 499het OHCs cannot be explained by simple summation of NLC parameters determined for WT and 499ki OHCs (Table 1 and Table 2), indicating that V_{pk} is not determined independently. Because the V_{pk} of prestin is known to be sensitive to membrane thickness likely due to hydrophobic mismatch (31), it is possible that voltage-dependent conformational change of WT-prestin affects the V_{pk} of 499-prestin in the same heteromer complex due to hydrophobic mismatch and vice versa. It is also interesting that the V_{pk} of 499het is significantly biased toward that of WT (Table 1). Recall that V_{pk} is defined as $\epsilon/z_{\mathrm{app}}e$ where ϵ is the conformational energy difference between the expanded and compacted states of prestin in the absence of an externally applied voltage. Using this definition, the V_{pk} of WT- and 499-prestin can be written as $\epsilon_{\mathrm{WT}}/z_{\mathrm{app,WT}}e$ and $\epsilon_{499}/z_{\mathrm{app,499}}e$, respectively. If WT- and 499-prestin form heteromers with equal stoichiometry, their respective V_{pk} is simply estimated as $(\epsilon_{\mathrm{WT}}+\epsilon_{499})/(z_{\mathrm{app,WT}}+z_{\mathrm{app,499}})/e$. Such computations have provided good estimates for WT-/Cl-prestin heteromers (−99 ± 14 mV predicted *versus* −94 ± 12 mV actual measurement; Ref. 32) and for D154N/D342Q prestin heteromers (−49 ± 14 mV predicted *versus* −43 ± 4 mV actual measurement; Ref. 12). Using this approach, the predicted V_{pk} of WT-/499-prestin heteromers based on the NLC parameters of WT and 499ki (Table 1) is +21 ± 25 mV. However, neither the observed V_{pk} of 499het OHCs (−66 ± 15 mV) (Table 1) nor the V_{pk} parameter determined for any dimer, trimer, or tetramer component (Table 2) is close to the predicted value of +21 mV. This discrepancy implies that the sensitivities of 499- and WT-prestin to membrane thickness may differ; *i.e.* 499-prestin may be more sensitive to membrane thickness (or hydrophobic mismatch) than WT-prestin. Sensitivity of the V_{pk} of prestin to the thickness of the cell membrane is in fact known to differ among different prestin orthologs (33). Therefore, it is possible that the V_{pk} sensitivity of prestin is altered by the V499G/Y501H mutation.

The current study also provides important insights regarding the motor mechanism of prestin. In this regard, it is interesting to point out that the NLC of WT-prestin measured using chloride (Fig. 6, *F* and *H*) showed a greater stimulus frequency dependence compared with that measured using iodide (Fig. 2, *A* and *C*). The significant increase ($p = 0.0056$) in the apparent electromechanical coupling efficiency of WT-prestin under the chloride condition (2.0 ± 0.6 nm/fC; Fig. 7*A*) compared with that determined under the iodide condition (1.4 ± 0.4 nm/fC; Fig. 7*B*) suggests that iodide better supports the fast motor action of prestin. Although different anions are known to affect the NLC of prestin in various degrees in terms of α, V_{pk}, and $Q_{\max}$ (6, 7, 26), their effects on motor kinetics have not been examined. Our study raises the possibility that changes in α and $Q_{\max}$ induced by some anions may be attributable to changes in motor kinetics. Therefore, characterizing anion effects in terms of the motor kinetics would be important in future studies for better defining the roles of anions in the energy transduction process of prestin.

The unique motor property of 499-prestin is now thought to relate to mutation of Val-499,which is highly conserved among SLC26 family members (Fig. 3), implying that Val-499 is fundamentally important for SLC26 proteins regardless of their phys-

iological roles as transporters or motors. Our study demonstrates the importance of the Val-499 site for retaining fast motor kinetics and the physiologically relevant voltage operating point of prestin. The important characteristic required for the Val-499 site seems to be high hydrophobicity (Fig. 4). Because the region is predicted to reside at the C-terminal end of the 12th transmembrane helix (Fig. 3), it is conceivable that the high hydrophobicity at the Val-499 site is required for this transmembrane helix to be stably embedded in the cell membrane, which may be essential for the fast motor action of prestin. The intermediate NLC phenotype seen in the Ala mutant (V499A) whose hydrophobicity is intermediate between Val and Gly is in good agreement with this scenario.

It is conceivable that the motor function of prestin evolved from an ancestral SLC26 transporter by modifying the transport mechanism to attain motor function (34). Such a possibility is supported by recent studies in which electromotile SLC26 proteins were generated by replacing portions of the non-electromotile SLC26 proteins with those of electromotile prestin (35–37). For example, Tan *et al.* (36) and Tang *et al.* (37) succeeded in converting non-electromotile SLC26 members into electromotile SLC26 members by swapping a very short non-charged amino acid segment. These results suggest that most if not all SLC26 proteins are potentially pre-equipped with the required molecular components to become motile, such as a voltage sensor(s) and an actuator(s). This possibility suggests that examination of the consequences of various mutations in other SLC26 transporters is important not only for defining their transport mechanisms but also for understanding the motor mechanism of prestin.

Acknowledgment—We are extremely grateful to an anonymous reviewer who suggested the possibility of altered kinetics as the basis of apparent change in coupling efficiency.

REFERENCES

1. Zheng, J., Shen, W., He, D. Z., Long, K. B., Madison, L. D., and Dallos, P. (2000) Prestin is the motor protein of cochlear outer hair cells. *Nature* **405,** 149–155
2. Liberman, M. C., Gao, J., He, D. Z., Wu, X., Jia, S., and Zuo, J. (2002) Prestin is required for electromotility of the outer hair cell and for the cochlear amplifier. *Nature* **419,** 300–304
3. Cheatham, M. A., Huynh, K. H., Gao, J., Zuo, J., and Dallos, P. (2004) Cochlear function in prestin knockout mice. *J. Physiol.* **560,** 821–830
4. Cheatham, M. A., Zheng, J., Huynh, K. H., Du, G. G., Edge, R. M., Anderson, C. T., Zuo, J., Ryan, A. F., and Dallos, P. (2007) Evaluation of an independent prestin mouse model derived from the 129S1 strain. *Audiol. Neurootol.* **12,** 378–390
5. Dallos, P., Wu, X., Cheatham, M. A., Gao, J., Zheng, J., Anderson, C. T., Jia, S., Wang, X., Cheng, W. H., Sengupta, S., He, D. Z., and Zuo, J. (2008) Prestin-based outer hair cell motility is necessary for mammalian cochlear amplification. *Neuron* **58,** 333–339
6. Rybalchenko, V., and Santos-Sacchi, J. (2003) Cl^- flux through a non-selective, stretch-sensitive conductance influences the outer hair cell motor of the guinea-pig. *J. Physiol.* **547,** 873–891
7. Rybalchenko, V., and Santos-Sacchi, J. (2008) Anion control of voltage sensing by the motor protein prestin in outer hair cells. *Biophys. J.* **95,** 4439–4447
8. Song, L., and Santos-Sacchi, J. (2010) Conformational state-dependent anion binding in prestin: evidence for allosteric modulation. *Biophys. J.* **98,** 371–376
9. Tan, X., Pecka, J. L., Tang, J., Okoruwa, O. E., Zhang, Q., Beisel, K. W., and He, D. Z. (2011) From zebrafish to mammal: functional evolution of prestin, the motor protein of cochlear outer hair cells. *J. Neurophysiol.* **105,** 36–44
10. Albert, J. T., Winter, H., Schaechinger, T. J., Weber, T., Wang, X., He, D. Z., Hendrich, O., Geisler, H. S., Zimmermann, U., Oelmann, K., Knipper, M., Göpfert, M. C., and Oliver, D. (2007) Voltage-sensitive prestin orthologue expressed in zebrafish hair cells. *J. Physiol.* **580,** 451–461
11. Zheng, J., Du, G. G., Anderson, C. T., Keller, J. P., Orem, A., Dallos, P., and Cheatham, M. (2006) Analysis of the oligomeric structure of the motor protein prestin. *J. Biol. Chem.* **281,** 19916–19924
12. Detro-Dassen, S., Schänzler, M., Lauks, H., Martin, I., zu Berstenhorst, S. M., Nothmann, D., Torres-Salazar, D., Hidalgo, P., Schmalzing, G., and Fahlke, C. (2008) Conserved dimeric subunit stoichiometry of SLC26 multifunctional anion exchangers. *J. Biol. Chem.* **283,** 4177–4188
13. Hallworth, R., and Nichols, M. G. (2012) Prestin in HEK cells is an obligate tetramer. *J. Neurophysiol.* **107,** 5–11
14. Mio, K., Kubo, Y., Ogura, T., Yamamoto, T., Arisaka, F., and Sato, C. (2008) The motor protein prestin is a bullet-shaped molecule with inner cavities. *J. Biol. Chem.* **283,** 1137–1145
15. Navaratnam, D., Bai, J. P., Samaranayake, H., and Santos-Sacchi, J. (2005) N-terminal-mediated homomultimerization of prestin, the outer hair cell motor protein. *Biophys. J.* **89,** 3345–3352
16. Zheng, J., Du, G. G., Matsuda, K., Orem, A., Aguiñaga, S., Deák, L., Navarrete, E., Madison, L. D., and Dallos, P. (2005) The C-terminus of prestin influences nonlinear capacitance and plasma membrane targeting. *J. Cell Sci.* **118,** 2987–2996
17. Cheatham, M. A., Zheng, J., Huynh, K. H., Du, G. G., Gao, J., Zuo, J., Navarrete, E., and Dallos, P. (2005) Cochlear function in mice with only one copy of the prestin gene. *J. Physiol.* **569,** 229–241
18. Homma, K., and Dallos, P. (2011) Evidence that prestin has at least two voltage-dependent steps. *J. Biol. Chem.* **286,** 2297–2307
19. Santos-Sacchi, J., Kakehata, S., and Takahashi, S. (1998) Effects of membrane potential on the voltage dependence of motility-related charge in outer hair cells of the guinea-pig. *J. Physiol.* **510,** 225–235
20. Homma, K., Miller, K. K., Anderson, C. T., Sengupta, S., Du, G. G., Aguiñaga, S., Cheatham, M., Dallos, P., and Zheng, J. (2010) Interaction between CFTR and prestin (SLC26A5). *Biochim. Biophys. Acta* **1798,** 1029–1040
21. Santos-Sacchi, J., and Navarrete, E. (2002) Voltage-dependent changes in specific membrane capacitance caused by prestin, the outer hair cell lateral membrane motor. *Pflugers Arch.* **444,** 99–106
22. Burnham, K. P., and Anderson, D. R. (2002) in *Model Selection and Multimodel Inference: a Practical Information-theoretic Approach*, 2nd Ed., pp. 60–64, Springer-Verlag, New York
23. Crooks, G. E., Hon, G., Chandonia, J. M., and Brenner, S. E. (2004) WebLogo: a sequence logo generator. *Genome Res.* **14,** 1188–1190
24. Ashmore, J. F. (1990) Forward and reverse transduction in the mammalian cochlea. *Neurosci. Res. Suppl.* **12,** S39–50
25. Santos-Sacchi, J. (1991) Reversible inhibition of voltage-dependent outer hair cell motility and capacitance. *J. Neurosci.* **11,** 3096–3110
26. Oliver, D., He, D. Z., Klöcker, N., Ludwig, J., Schulte, U., Waldegger, S., Ruppersberg, J. P., Dallos, P., and Fakler, B. (2001) Intracellular anions as the voltage sensor of prestin, the outer hair cell motor protein. *Science* **292,** 2340–2343
27. Pasqualetto, E., Aiello, R., Gesiot, L., Bonetto, G., Bellanda, M., and Battistutta, R. (2010) Structure of the cytosolic portion of the motor protein prestin and functional role of the STAS domain in SLC26/SulP anion transporters. *J. Mol. Biol.* **400,** 448–462
28. Shelden, M. C., Howitt, S. M., and Price, G. D. (2010) Membrane topology of the cyanobacterial bicarbonate transporter, BicA, a member of the SulP (SLC26A) family. *Mol. Membr. Biol.* **27,** 12–23
29. Tadenuma, T., Iida, K., and Murakoshi, M. (2008) Functional expression of prestin, the outer hair cell motor protein, using the baculovirus/insect cell system. *J. Biomech. Sci. Eng.* **3,** 287–298
30. Wang, X., Yang, S., Jia, S., and He, D. Z. (2010) Prestin forms oligomer with four mechanically independent subunits. *Brain Res.* **1333,** 28–35

31. Fang, J., Izumi, C., and Iwasa, K. H. (2010) Sensitivity of prestin-based membrane motor to membrane thickness. *Biophys. J.* **98,** 2831–2838
32. Gao, J., Wang, X., Wu, X., Aguinaga, S., Huynh, K., Jia, S., Matsuda, K., Patel, M., Zheng, J., Cheatham, M., He, D. Z., Dallos, P., and Zuo, J. (2007) Prestin-based outer hair cell electromotility in knockin mice does not appear to adjust the operating point of a cilia-based amplifier. *Proc. Natl. Acad. Sci. U.S.A.* **104,** 12542–12547
33. Izumi, C., Bird, J. E., and Iwasa, K. H. (2011) Membrane thickness sensitivity of prestin orthologs: the evolution of a piezoelectric protein. *Biophys. J.* **100,** 2614–2622
34. Elgoyhen, A. B., and Franchini, L. F. (2011) Prestin and the cholinergic receptor of hair cells: positively-selected proteins in mammals. *Hear. Res.* **273,** 100–108
35. Schaechinger, T. J., Gorbunov, D., Halaszovich, C. R., Moser, T., Kügler, S., Fakler, B., and Oliver, D. (2011) A synthetic prestin reveals protein domains and molecular operation of outer hair cell piezoelectricity. *EMBO J.* **30,** 2793–2804
36. Tan, X., Pecka, J. L., Tang, J., Lovas, S., Beisel, K. W., and He, D. Z. (2012) A motif of eleven amino acids is a structural adaptation that facilitates motor capability of eutherian prestin. *J. Cell Sci.* **125,** 1039–1047
37. Tang, J., Pecka, J. L., Tan, X., Beisel, K. W., and He, D. Z. (2011) Engineered pendrin protein, an anion transporter and molecular motor. *J. Biol. Chem.* **286,** 31014–31021